J Mater Sci (2008) 43:2889–2894
DOI 10.1007/s10853-007-1924-z

Effect of mechanical coating with Ni and Ni–5% Al on the structure and electrochemical properties of the Mg–50% Ni alloy

Sydney Ferreira Santos · José Fernando R. de Castro · Tomaz T. Ishikawa · Edson A. Ticianelli

Received: 29 November 2006 / Accepted: 6 June 2007 / Published online: 28 July 2007

Abstract The Mg–Ni metastable alloys (with amorphous or nanocrystalline structures) are promising candidates for anode application in nickel–metal hydride rechargeable batteries due to its large hydrogen absorbing capacity, low weight, availability, and relative low price. In spite of these interesting features, improvement on the cycle life performance must be achieved to allow its application in commercial products. In the present paper, the effect of mechanical coating of a Mg–50 at.% Ni alloy with Ni and Ni–5 at.% Al on the structure, powder morphology, and electrochemical properties is investigated. The coating additives, Mg–Ni alloy and resulting nanocomposites (i.e., Mg–Ni alloy + additive) were investigated by means of X-ray diffraction and scanning electron microscopy. The Mg–Ni alloy and nanocomposites were submitted to galvanostatic cycles of charge and discharge to evaluate their electrode performances. The mechanical coating with Ni and Ni–5% Al increased the maximum discharge capacity of the Mg–Ni alloy from of 221 to 257 and 273 mA h g^{-1}, respectively. Improvement on the cycle life performance was also achieved by mechanical coating.

S. F. Santos · J. F. R. de Castro · E. A. Ticianelli
Institute of Chemistry of São Carlos, University of São Paulo, Av. Trab. São-carlense, 400, C.P. 780, Sao Carlos, SP CEP: 13560-970, Brazil

T. T. Ishikawa
Department of Materials Engineering, Federal University of São Carlos, Rod. Washinghton Luiz, Km 235, Sao Carlos, SP CEP: 13565-905, Brazil

Present Address:
S. F. Santos (✉)
Institut de Recherche sur l'Hydrogène, Université du Québec à Trois-Rivières, 3351 des Forges, P.O. Box 500, Trois-Rivieres, QC, Canada G9A5H7
e-mail: sfsantos91@yahoo.com.br

Introduction

Since 1989, nickel–metal hydride (Ni–MH) rechargeable batteries have been commercially produced [1]. These batteries have 50% higher volumetric and gravimetric energy densities than conventional Ni–Cd ones. Another interesting aspect of Ni–MH batteries is the absence of Cd, a very toxic element [2, 3]. In spite of these advantages, new developments on portable electronic devices and miniaturization create a demand for batteries with larger energy densities than the actual available in the market. Researches addressing the development of novel Ni–MH batteries with improved capacities have been extensively performed trying to satisfy these needs. Among others, Mg–Ni alloys appear as promising candidate materials for anode applications due to its large hydrogen absorbing capacities, low cost and low weight [4]. The Mg–Ni alloys with metastable (amorphous and/or nanocrystaline) structures exhibit large discharge capacities, usually achieved in the first cycle. To obtain these structures, these alloys are generally synthesized by mechanical alloying [4–6]. On the other hand, there are major problems that must be overcome to make possible the technological application of these alloys on batteries. The main drawback to the use of Mg–Ni alloy electrodes is the low stability of Mg in the presence of an alkaline electrolyte. This undesirable feature is responsible by the accentuated decay of the discharge capacities in Mg–Ni alloys after few cycles of charge/discharge [4–6]. Some strategies addressed to increase the

cycle life performance of these alloy electrodes have been investigated and presented positive results in some extent. The main strategies currently investigated are: (a) addition of alloying elements, mainly transition (Cu, Zr, Ti, etc.) and noble (Pd and Pt) metals [4–10]; (b) elaboration of composite materials between Mg–Ni and other alloys or compounds [11–13]; and (c) coating (microencapsulation) of Mg–Ni particles with metallic elements such as Cu, Ni and Pd [14–16].

Investigations concerning coating of electrode materials have been frequently reported for AB_5 and AB_2-type intermetallics [17–23] but there are also some studies for Mg–Ni alloys [24–27]. Among others, Ni seems to be a suitable coating element for Mg–Ni alloys due to its stability in alkaline solution, high electro-catalytic activity and low price when compared to noble metals, such as Pd. The coating of hydrogen absorbing alloys is usually carried out by electroless deposition [15, 17–25]. Nevertheless, it can be performed by other techniques such as decomposition of a precursor in supercritical fluid [16] or mechanical coating, i.e. ball-milling the alloy with an additive (coating materials) during short times [14].

Taking into account that Mg–Ni alloys investigated for electrode applications are usually synthesized by mechanical alloying, the mechanical coating appears as an attractive way to produce coated particles since it will only imply in one more step of processing (i.e., add the coating material to the ball-milled alloy and promote its dispersion on the particles surface). In the present work, it was investigated the effect of mechanical coating on the structure and electrode performance of the Mg–50 at.% Ni alloy. The investigated additives were Ni and Ni–5% Al powders. The additives, Mg–Ni alloy and final nanocomposites (alloy + additives) were characterized by X-ray diffraction (XRD) and scanning electron microscopy (SEM). The electrochemical characterization was carried out by galvanostatic cycles of charge and discharge.

Experimental procedure

The additives (Ni and Ni–5 at.% Al) and metallic matrix (Mg–50 at.% Ni alloy) were synthesized by high energy ball-milling for 12 and 72 h, respectively. The mass to powder weight ratio was 15:1. After this first step, two nanocomposite materials were synthesized by mixing 5 wt.% of additive with the Mg–Ni alloy. These powders (MgNi alloy + additive) were then milled for 1 h to promote their homogeneous distribution. All millings were carried out using a Fritsch P7 planetary ball-mill under argon atmosphere.

The structural characterization was performed by XRD using a Siemens D5005 diffractometer, with Cu-K_α radiation and the morphology of the powders was analyzed by secondary electrons (SE) in the SEM using a Zeiss DSM 940 microscope.

For the electrochemical tests, the working electrodes were prepared by cold pressing a mixture of 0.1 g of the sample with 0.1 g of a blend of carbon black (Vulkan XC-72R) with 33 wt.% of polytetrafluoroethylene (PTFE) binder in both sides of a Ni screen with 2 cm^2 of area. The electrochemical measurements were carried out in a three electrode cell, with a Pt counter electrode, an Hg/HgO reference electrode and a 6 mol L^{-1} KOH electrolyte. The density of charge of the electrodes was 200 mA g^{-1} of active material and the discharge density was 20 mA g^{-1}. The cut-off potential was –0.65 V (versus Hg/HgO, KOH-6 mol L^{-1}).

Results and discussions

Figures 1 and 2 show the SE-SEM images of the Ni–5% Al and Ni powders, respectively, after 12 h of milling. It can be observed the presence of two types of morphology in both powders: (i) small agglomerates of fine and rounded particles, in small quantity, and (ii) large flattened agglomerates with platelet shapes, which are the majority. These morphological features are caused by predominance of deformation and cold welding of the particles instead of fracture, which is typical during the initial states of ball-milling for ductile metallic systems [25].

The SEM image of the Mg–Ni alloy, after 72 h of ball-milling, is shown in Fig. 3. This powder is composed by agglomerates, in the range of 5 μm of diameter, of fine particles with diameters smaller than 1 μm. Differences between the morphology of additives and Mg–Ni alloy should be attributed to the different milling times and also

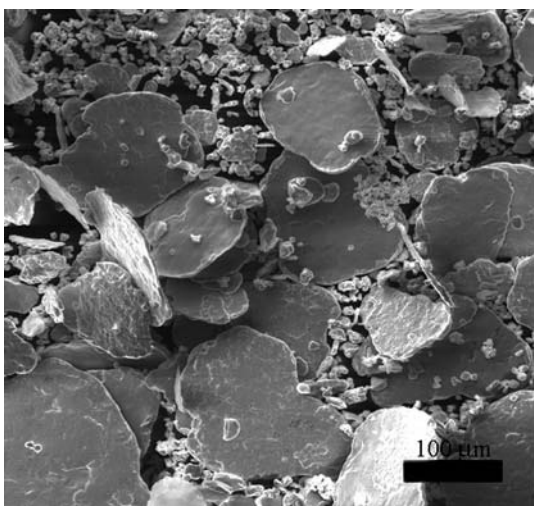

Fig. 1 SEM image of the Ni–5 at.% Al additive after 12 h of ball-milling

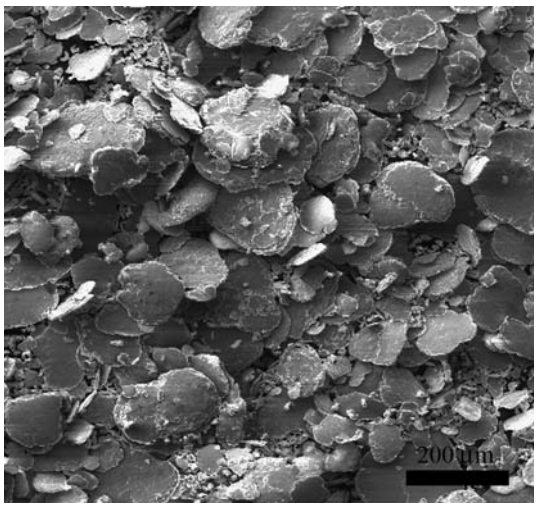

Fig. 2 SEM image of the Ni additive after 12 h of ball-milling

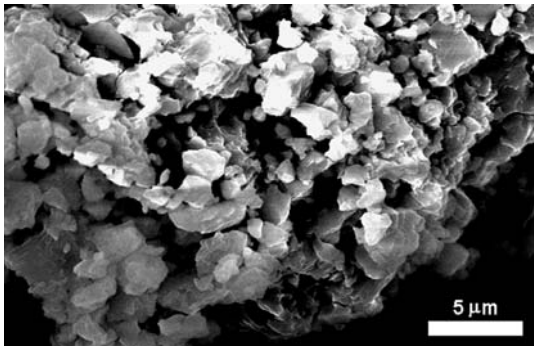

Fig. 3 SEM image of the Mg–50 at.% Ni alloy after 72 h of ball-milling

to the difference in chemical compositions. One of the additives is pure Ni and the other one is Ni with only 5 at.% of Al and, consequently, present larger ductility when compared to the Mg–50 at.% Ni alloy, due to the absence (in the case of Ni) or small effect (in the case of Ni–5% Al) of solution hardening and, for both additives, absence of precipitation hardening, leading to the predominance of deformation and cold welding even after 12 h of milling. On the other hand, in the case of Mg–Ni alloys, the equiatomic ratio between the elements and longer milling times favored alloy hardening and formation of intermetallics, leading to predominance of fracture rather than cold welding.

Figures 4 and 5 show the SEM images of (Mg–Ni) + 5% Ni and (Mg–Ni) + 5% (Ni–Al) nanocomposites, respectively. Both nanocomposites present similar morphologies, been composed by agglomerates of fine spherical particles. It is not observed flattened agglomerates with platelet shapes, like the as-milled additives. This feature could be associated to the small amount (5 wt.%) and homogeneous distribution of additives on the Mg–Ni particles surface.

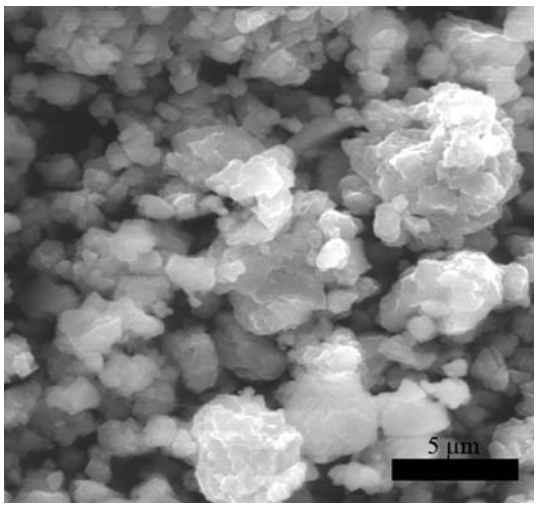

Fig. 4 SEM image of the (Mg–50 at.% Ni) + 5 wt.% Ni nanocomposite

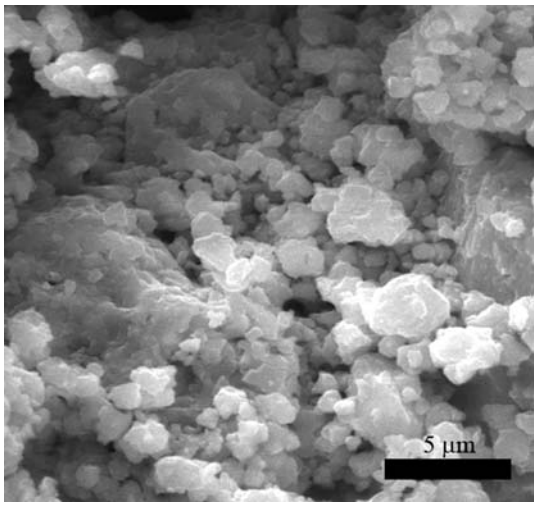

Fig. 5 SEM image of the (Mg–50 at.% Ni) + 5 wt.% (Ni–5 at.% Al) nanocomposite

Figure 6 shows the XRD patterns of Ni and Ni–5 at.% Al additives after ball-milling. It can be observed some broadening of the diffraction peaks due to the strain and/or crystallite size reduction promoted by milling. These results match with SEM images (Figs. 1, 2) that showed the deformed aspect of the additive particles. The Ni (111) diffraction peak shifted to a lower 2θ when alloyed with Al, indicating an increase in the FCC lattice parameter. This result indicates the formation of a Ni–Al solid solution. The lattice parameters of Ni and Ni–5% Al, after ball milling, are 3.5119 and 3.5235 Å, respectively. The presence of a small diffraction peak of Al phase in the Ni–Al diffraction pattern indicates that Al was only partially inserted into the Ni metallic matrix, remaining some amount unalloyed. Assuming a linear variation of the lattice parameter of Ni as a function of the Al content, it

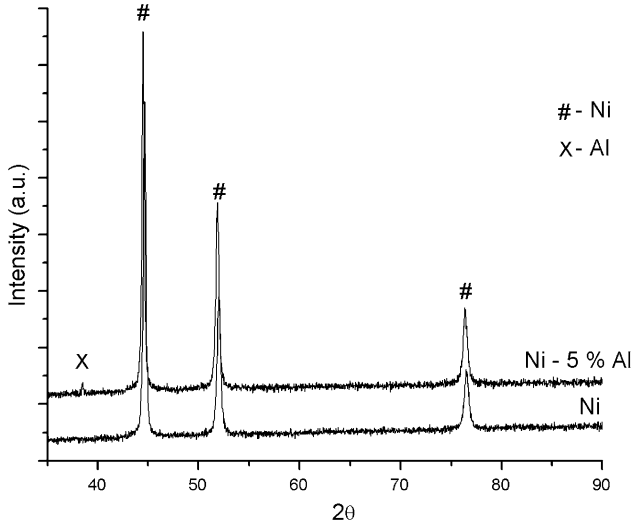

Fig. 6 XRD patterns of Ni and Ni–5 at.% Al additives

can be estimated that approximately 2.2 at.% of Al formed a solid solution with Ni. The partial alloying between Ni and Al, indicated by the XRD results, is in good agreement with the SEM image (Fig. 1) since the observed morphology is typical of initial stages of mechanical alloying in ductile systems, when the elements are not completely mixed in atomic level [25].

The XRD patterns of the Mg–Ni, (Mg–Ni) + 5 wt.% Ni and (Mg–Ni) + 5 wt.% (Ni–Al) are shown in Fig. 7. As expected, it was only observed diffraction peaks of the Mg_2Ni and $MgNi_2$ phases. These peaks are largely broadened due to crystallite size reduction and strain in the sample after 72 h of ball-milling. The presence of an amorphous band overlapped with the diffraction peaks is also suggested. For the nanocomposite samples, the diffraction peaks are less defined due to an increase in the broadening and decrease of relative intensity. Two diffraction peaks of the Mg_2Ni phase, which are clearly detected in the Mg–Ni alloy (at $2\theta = 37.2°$ and 40°, respectively), are almost not observed in the XRD patterns of the nanocomposites. Both SEM and XRD of the nanocomposites indicate refined morphology with small particle and crystallite sizes.

Figure 8 shows the curves of discharge capacity (mA h g^{-1}) versus number of cycles for the investigated materials. All samples presented the maximum discharge capacity in the first cycle, indicating the activated state of the samples. This initial high activity of ball-milled Mg–Ni alloy electrodes has been reported by several authors [2–8], besides increasing of the discharge capacity during the first cycles (activation) was reported for $Mg_{67}Ni_{23}Pd_{10}$ melt-spun alloy electrode [26].

Further cycles promoted decay in these curves. The maximum discharge capacity achieved by the Mg–Ni alloy

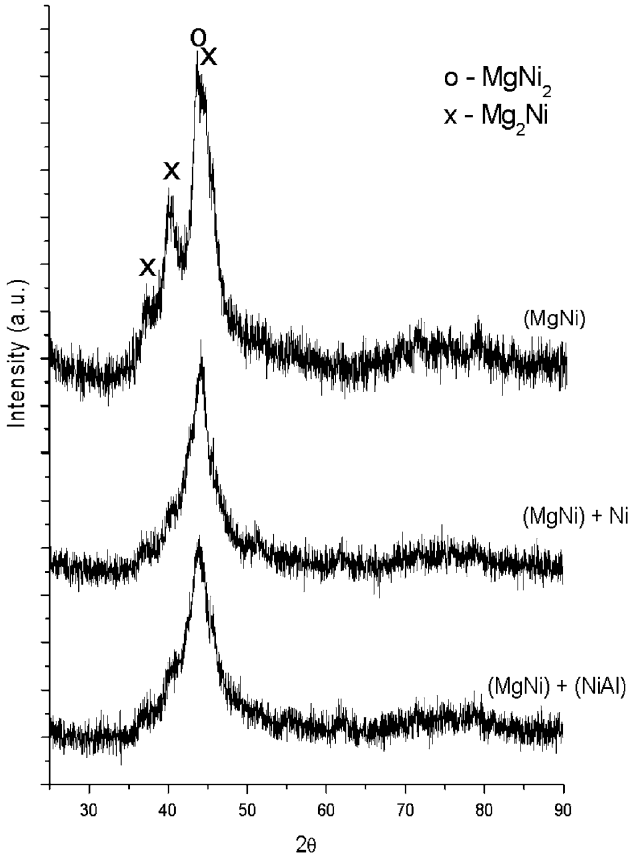

Fig. 7 XRD patterns of the Mg–50% Ni alloy and nanocomposites

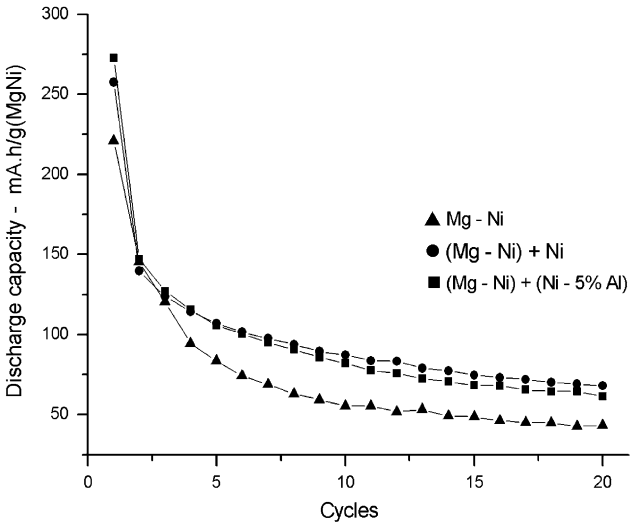

Fig. 8 Curves of discharge capacity × number of cycles of the Mg–Ni alloy and nanocomposites

was 221 mA h g^{-1}. The mechanical coating with Ni and Ni–5% Al increased this capacity to 257 and 273 mA h g^{-1}, respectively. The values of initial discharge capacity for the Mg–50% Ni alloy reported on the literature are in the range of 200 up to 500 mA h g^{-1} [4–10, 24, 27–29]. This large spread

is due to several reasons like: (i) processing parameters adopted to synthesize the alloy (type of mill, ball-to-powder weight ratio, time of milling, etc.); (ii) structural features of the obtained alloy (phases formed, particles size, crystallite size, etc); (iii) electrochemical parameters adopted for the tests (density of charge, density of discharge, cut-off potentials, etc). In the present investigation, the relative low value obtained for the maximum discharge capacity of the Mg–Ni alloy should be mainly related to the presence of crystalline phases, since the higher values have been reported for alloys with fully amorphous structures.

Table 1 presents the values of retained capacities, i.e. the ratio between the discharge capacity in the *n*th cycle (C_n) and maximum discharge capacity (C_{max}), for the investigated alloy and nanocomposites. Both, maximum discharge capacity and durability of the electrodes were improved after mechanical coating.

After 20th cycles, the retained capacity of the electrodes were 19.6%, 22.5% and 26.5% for Mg–50% Ni, (Mg–Ni) + (Ni–5% Al) and (Mg–50% Ni) + Ni, respectively. Beside the values achieved by the nanocomposites are not enough to make possible the practical application of these electrodes, it shows a clear tendency of improvement of the electrode performances with coating. The fast degradation of the of the Mg–Ni-based alloy electrodes is mainly related to the formation of $Mg(OH)_2$ on the surface of the particles, hindering the charge transfer reaction [4, 5]. Goo et al. [14] reported that the retained capacity of the ball milled Mg_2Ni increased five times after mechanical coating with Ni. On the other hand, the maximum discharge capacity achieved by these authors was almost the same for the coated and uncoated electrodes (180 mA h g^{-1}, approximately). Pasturel et al. [16] reported the increase in the discharge capacity for the Mg–50% Ni alloy after coating with Cu (from 240 to 260 mA h g^{-1}). The degradation kinetics of the electrodes, reported by these authors, is also similar with those obtained in the present work. After 12 cycles, the retained discharge capacity of the Cu coated electrode was 37%. In the present investigation, the retained capacities after the same number of cycles were 28% and 32% for Ni–5% Al and Ni coatings, respectively. Rongeat et al. [24] investigated the electroless deposition of chromate coating on the Mg–50 at.% Ni alloy. These authors reported a decrease in the initial discharge capacity of the alloy electrode of roughly 14% after coating. In the coated alloy electrode, the discharge capacity after two cycles remained constant but started to decay thereafter reaching 50% of remaining capacity in the 12th cycle. These authors suggested a rupture of the chromate coating due to the stress generation and pulverization, caused by the large variation of volume during the hydride formation and decomposition, as the main responsible for the decay of discharge capacity. On the other hand, the coating of AB_5 alloy electrodes presents better electrochemical results, as reported by several authors [17–23]. Rongeat and co-authors considered that a lower stress-cracking in the AB_5 alloys could be the cause for this higher effectiveness [24]. Nevertheless, it is important to note the existence of significant volume expansion during hydride formation in $LaNi_5$ compound ($\Delta V/V$ = 24.9%) [30].

Table 1 Retained capacity of the electrodes

Samples	C5th (%)	C10th (%)	C20th (%)
Mg–Ni	37.7	25.1	19.6
(Mg–Ni) + (Ni–Al)	38.7	30.1	22.5
(Mg–Ni) + Ni	41.6	30.2	26.5

In the case of mechanical coating, a homogeneous dispersion of the additive on the particles surface alloy is obtained but there is not achieved a dense and compact coating fully recovering the particles, like in the case of deposition methods. This difference suggests that mechanical coating could have a smaller sensibility to the volume expansion (contraction) due to hydride formation (decomposition) [24].

Although the cycle life performance obtained after mechanical coating cannot be considered satisfactory, they indicate that a partial protection of the Mg–Ni particles occurred, resulting in decrease of the degradation kinetics of electrodes. These results also suggest that further improvements on the cycle life performance of the coated electrodes could be achieved by optimizing the processing parameters of the nanocomposite powders, such as amount of additive, milling time, etc. Another approach to optimize the electrodes performance of Mg–Ni alloys is the adoption of more than one technique to reduce its degradation kinetics as, for example, addition of alloying elements (i.e., elaboration of ternary or quaternary alloys) and the mechanical coating. Rongeat et al. [24] adopted this approach of multiple techniques for optimizing an Mg–Ni alloy electrode. These authors combined the: (i) addition of transition metals (synthesizing a quaternary Mg–Ni–Ti–Al alloy), (ii) control of the particles size and (iii) limit of the input charge, obtaining better results than those obtained when these techniques of optimization were adopted individually.

Conclusions

The mechanical coating with Ni and Ni–5% Al improved both maximum discharge capacity and cycle life of the Mg–50 at.% Ni alloy electrode. The initial discharge capacity increased from 221 mA h g^{-1} to 257 and 273 mA h g^{-1} and the retained capacity after 20 cycles increased from 19 to 26 and 22% after mechanical coating

with Ni and Ni–5% Al additives, respectively. These positive electrochemical results obtained after mechanical coating are not sufficient to make possible the practical application of these electrodes but clearly indicate that a partial protection of the Mg–Ni particles was accomplished. Investigations on the optimization of the processing parameters of mechanical coating are still necessaries to achieve further improvement of the electrodes performance.

Acknowledgements The authors would like to thank the Brazilian institutions FAPESP and CNPq for the financial support of this research.

References

1. Ovshinsky SR, Fetcenko MA (2001) Appl Phys A 72:239
2. Fetcenko MA, Ovshinsky SR, Reichman B, Young K, Fierro C, Zallen A, Mays W, Ouchi T (2007) J Power Sources 165:544
3. Notten PHL, Ouwerkerk M, van Hal H, Beelen D, Keur W, Zhuo J, Feil H (2004) J Power Sources 124:45
4. Jiang JJ, Gasik M (2000) J Power Sources 89:117
5. Han S-C, Lee PS, Lee J-Y, Zuttel A, Schlapbach L (2000) J Alloys Comp 306:219
6. Lee HY, Goo NH, Jeong WT, Lee KS (2000) J Alloys Comp 313:258
7. Santos SF, de Castro JFR, Ishikawa TT, Ticianelli EA (2007) J Alloys Comp 434–435:756
8. Ye H, Lei YQ, Chen LS, Zhang H (2000) J Alloys Comp 311:194
9. Souza EC, de Castro JFR, Ticianelli EA (2006) J Power Sources 160:1425
10. Ruggeri S, Roué L, Huot J, Schulz R, Aymard L, Tarascon J-M (2002) J Power Sources 112:547
11. Wang FX, Gao XP, Lu ZW, Ye SH, Qu JQ, Wu F, Yuan HT, Song DY (2004) J Alloys Comp 370:326
12. Choi W-K, Tanaka T, Miyauchi R, Morikawa T, Inoue H, Iwakura C (2000) J Alloys Comp 299:141
13. Cui N, Luo JL (1998) Electrochem Acta 44:711
14. Goo NH, Woo JH, Lee KS (1999) J Alloys Comp 288:286
15. Wang CY, Yao P, Bradhurst DH, Liu HK, Dou SX (1999) J Alloys Comp 285:267
16. Pasturel M, Bobet JL, Chevalier B (2003) J Alloys Comp 356:764
17. Wu M-S, Wu H-R, Wang Y-Y, Wan C-C (2000) J Alloys Comp 302:248
18. Wu M-S, Wu H-R, Wang Y-Y, Wan C-C (2004) Int J Hydrogen Energy 29:1263
19. Barsellini D, Visitin A, Triaca WE, Soriaga MP (2003) J Power Sources 124:309
20. Deng C, Shi P, Zhang S (2006) Mater Chem Phys 98:514
21. Ambrosio RC, Ticianelli EA (2005) Surf Coat Technol 197:215
22. Ambrosio RC, Ticianelli EA (2005) J Electroanal Chem 574:251
23. Feng F, Northwood DO (2004) Int J Hydrogen Energy 29:955
24. Rongeat C, Grosjean M-H, Ruggeri S, Dehmas M, Bourlot S, Marcotte S, Roué L (2006) J Power Sources 158:747
25. Suryanarayana C (2001) Prog Mater Sci 46:1
26. Yamaura S-I, Kim H-Y, Kimura H, Inoue A, Arata Y (2002) J Alloys Comp 347:239
27. Liu J-W, Yuan H-T, Cao J-S, Wang Y-J (2005) J Alloys Comp 329:300
28. Ma T, Hatano Y, Abe T, Watanabe K (2004) J Alloys Comp 372:251
29. Zhang SG, Hara Y, Morikawa T, Inoue H, Iwakura C (1999) J Alloys Comp 293–295:552
30. Joubert J-M, Černý R, Latroche M, Percheron-Guégan A, Schmitt B (2006) Acta Mater 54:713